

Strong coupling of alkali spins to noble-gas spins with hour-long coherence time

R. Shaham,^{1,2,*} O. Katz,^{1,2,3,*} and O. Firstenberg¹

¹*Department of Physics of Complex Systems, Weizmann Institute of Science, Rehovot 76100, Israel*

²*Rafael Ltd, IL-31021 Haifa, Israel*

³*Present address: Department of Electrical and Computer Engineering, Duke University, Durham, NC 27708*

Nuclear spins of noble gases can maintain coherence for hours at ambient conditions owing to their extraordinary isolation by the enclosing, complete electronic shells [1]. This isolation, however, impedes the ability to manipulate and control them by optical means or by physical coupling to other spin gases [2–4]. Here we experimentally achieve strong coherent coupling between noble-gas spins and the optically-accessible spins of alkali-metal vapor. Stochastic spin-exchange collisions, underlying the coupling, accumulate to a coherent periodic exchange of spin excitations between the two gases. We obtain a coupling rate 10 times higher than the decay rate, observe the resultant avoided crossing in the spectral response of the spins, and demonstrate the external control over the coupling by magnetic fields. These results open a route for efficient and rapid interfacing with noble-gas spins for applications in quantum sensing and information [5, 6].

INTRODUCTION

Noble gas isotopes with a nonzero nuclear spin, such as helium-3, feature day-long spin lifetimes and hours-long coherence times [1, 7]. They are prominent in various fields, from precision sensing [8–11] and medical imaging [12] to searches of new physics [13–17], and they hold promise for future quantum information applications such as optical quantum memories and generation of long-lived entanglement [5, 18–20]. The latter rely on the feasibility of preparing the collective spin state of the gas and controlling its quantum excitations [21].

Polarized ensembles of alkali-metal spins or noble-gas spins can carry such collective excitations, corresponding classically to a tilt of the collective spin about the polarization axis [22]. These can be modeled as quantum excitations of a harmonic oscillator. Remarkably, the quantum description persists even for gaseous ensembles undergoing rapid diffusion [23, 24] and for overlapping ensembles that interact via atomic collisions [21, 25–27]. The collective state of alkali spins can be addressed and coherently controlled by optical means [28–30]. The same, however, cannot be done for the nuclear spins of noble gases, which lack any optical transition from the ground levels. Instead, one can access the noble-gas spins by collisions with another spin gas, either excited (metastable) helium-3 or alkali vapor, both of which possess optically-accessible spins [1, 31, 32]. Alkali atoms exchange spin with noble-gas atoms via a weak electron-nuclear coupling (Fermi contact) during collisions [33]. They are normally used for hyperpolarizing the noble gas and for probing its spin dynamics. The probing relies on the coherent component of the spin-exchange interaction, which is usually weak and manifests as a shift in the precession frequencies of the alkali spins. It is employed for readout of noble-gas-based sensors and for inherent suppression of sensitivity to magnetic fields [2–4, 9]. Recently, we used alkali spins as off-resonant mediators to couple light to noble-gas spins bidirectionally [34]. However, these works have been limited to the regime of detuned or overdamped coupling, with the alkali spin relaxation exceeding the coupling strength to the

noble-gas spins.

Here we report on strong coherent coupling between the collective spin states of noble-gas and alkali ensembles. We enter the strong-coupling regime by reaching high polarizations and densities of the interacting species while minimizing spin relaxation. We directly probe the dynamics of both spin ensembles and demonstrate the coherent exchange of excitations between them in the temporal domain as well as the corresponding gap between the normal frequencies of the coupled system in the spectral domain. These results certify that stochastic spin-exchange collisions that are individually weak but altogether frequent enough can accumulate to form an efficient coherent interface between two spin gases.

Consider the bosonic, collective, spin excitations of the alkali and noble-gas spins, represented by the annihilation operators \hat{a} and \hat{b} , respectively. The coupling between these excitations relies on the collective enhancement of the exchange interaction, due to accumulation of numerous collisions among the two spin ensembles. The collective, bi-directional, coupling rate $J = (\tilde{\zeta}/2)\sqrt{n_a p_a n_b p_b}$ thus depends on the square root of the atomic densities n_a , n_b and degrees of polarization $0 \leq p_a, p_b \leq 1$ [21]. The microscopic coupling strength $\tilde{\zeta}(p_a)$, incorporating the collisional cross-section, has a weak dependence on the alkali spin polarization due to the hyperfine structure of the alkali atoms (see Methods). A simple form of two coupled modes can be used to describe the exchange dynamics,

$$\partial_t \begin{pmatrix} \hat{a} \\ \hat{b} \end{pmatrix} = i \begin{pmatrix} \omega_a + i\gamma & -J \\ -J & \omega_b \end{pmatrix} \begin{pmatrix} \hat{a} \\ \hat{b} \end{pmatrix} + \hat{f}. \quad (1)$$

Here ω_a and ω_b denote the Larmor precession frequencies of the collective spins of the alkali and noble-gas atoms, respectively. They are set by the external magnetic field B and by the effective magnetic fields exerted by each species on the other [31]. We tune B to determine the detuning from resonant couplings $\Delta = \omega_a - \omega_b$. The decoherence rate of the alkali excitations γ is included, while for now we neglect the slow decoherence of the noble-gas spins. Finally, \hat{f} denotes the quantum noise accompanying the relaxation, motion, and

collision processes [21, 23]. In the current study, \hat{f} can be discarded, as we prepare the spin ensembles in coherent spin states and study the evolution of the mean transverse amplitudes $\langle \hat{a} \rangle$ and $\langle \hat{b} \rangle$.

When $J > \gamma$, Eq. (1) describes the exchange of spins at a rate $\tilde{J} \approx \sqrt{J^2 + \Delta^2/4}$ and with a contrast $(J/\tilde{J})^2$, in a frame rotating at ω_b . Strong coupling is achieved for $J > \{\gamma, \Delta\}$, which produces exchange oscillations with near-unity contrast.

RESULTS

Experimental setup and protocols

We study transverse spin excitations of polarized potassium vapor and helium-3 gas enclosed in a spherical glass cell, as shown in Fig. 1a. The potassium spins are polarized along the axial magnetic field by an optical pumping beam, and the helium spins are polarized by collisions with the polarized potassium (over 10 hours, see Fig. 5). The cell also contains nitrogen for reducing (quenching) the fluorescence from the optically excited potassium atoms. At a low polarization, the helium spins exhibit a coherence time of $T_2^b = 2$ hours, as shown in Fig. 1b, and consequently their individual relaxation is henceforth neglected. The exchange experiments start with turning off the pumping beam.

We monitor the dynamics of the coupled spin system following a short, 5- μs -long pulse of transverse magnetic field B_{\perp} , which predominantly excites the collective alkali spin and initializes it at a tilt angle of a few degrees from the axial magnetic field B_z . We measure the transverse alkali spin using Faraday rotation of an optically-detuned, linearly-polarized probe beam. We perform a tomographic-like reconstruction of the alkali spin in the xy plane by alternating between $B_{\perp}\hat{y}$ and $B_{\perp}\hat{x}$ for initialization. We properly scale these measurements by the total degree of polarization $p_a(t)$ (measured independently, see Fig. 7) and calculate the complex amplitude of the collective alkali spin $\langle \hat{a}(t) \rangle$. To measure the collective noble-gas spin $\langle \hat{b}(t) \rangle$ after some exchange duration t , we halt the exchange dynamics at t by rapidly ramping up the axial magnetic field (increasing Δ) and utilizing the alkali spins as a magnetometer for sensing the noble-gas spin precession.

We realize a maximal coupling rate of $J = 78 \pm 8$ Hz by operating at high densities of potassium $n_a = 4.9 \cdot 10^{14}/\text{cc}$ (at $T = 230$ °C) and helium $n_b = 6.45 \cdot 10^{19}/\text{cc}$ (2.4 atm at room temperature) and with relatively high degrees of spin polarization $p_a \gtrsim 0.95$ and $p_b \gtrsim 0.3$. At these conditions, collisions among alkali atoms are frequent enough ($> 0.5/\mu\text{s}$) with respect to the Larmor frequency to keep the alkali excitations free from spin-exchange relaxation (so-called SERF regime) [31]. The intricate hyperfine manifold of the alkali atoms maintains a spin-temperature distribution due to these collisions and manifests as an effective spin-1/2, as shown in Fig. 1c [31]. Remnant spin-relaxation occurring

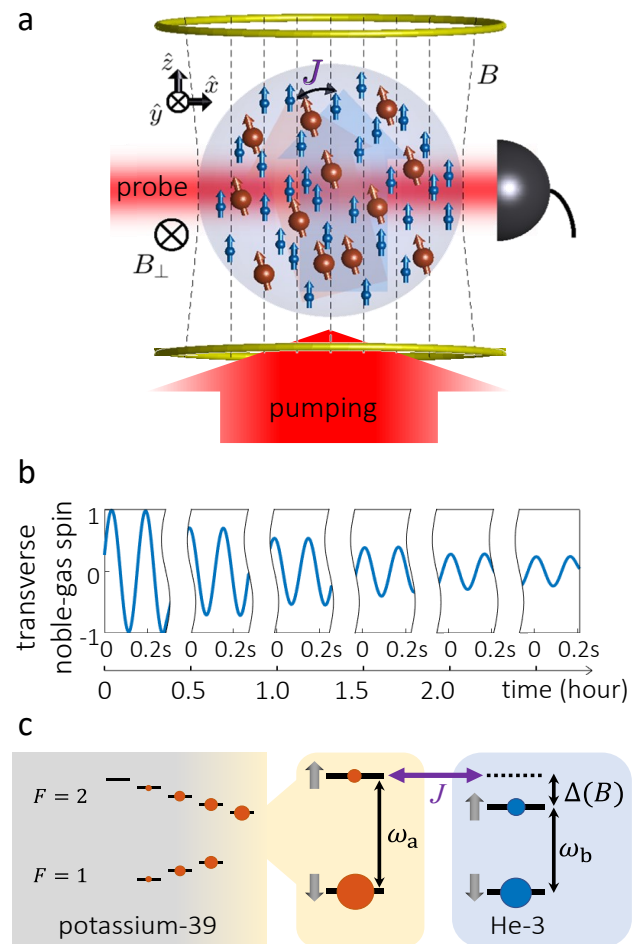


FIG. 1. Experimental scheme and coherence-time measurements. **a.** A glass cell containing optically-pumped potassium vapor (alkali spins, red) and helium-3 (noble-gas spins, blue). The polarized ensembles couple via stochastic atomic collisions that accumulate to a collective spin-exchange interaction at a rate J . An applied magnetic field B_z controls the precession frequency difference $\Delta = \omega_a - \omega_b$ between the two ensembles. A transverse excitation of the spins is initialized by a short transverse magnetic field pulse $B_{\perp}\hat{y}$ and then monitored by Faraday rotation of an optical probe. **b.** Precession of the helium-3 spins, measured at low spin polarizations and normalized to the initial value, featuring a coherence time of $T_2^b = 2$ hours. **c.** Energy level diagram for the coupled spins. The spin-polarized alkali atoms, undergoing frequent spin-exchange collisions, can be described as an effective two-levels system.

during these collisions dominates the decoherence rate of the alkali excitations $\gamma = 6 \pm 1.5$ Hz. We thus achieve $J \gtrsim 10\gamma$. See Methods for a detailed description of the experimental conditions and analysis procedures.

Dynamics of strongly-coupled spins

Under the strong-coupling conditions, the two spin gases can coherently exchange collective excitations. To

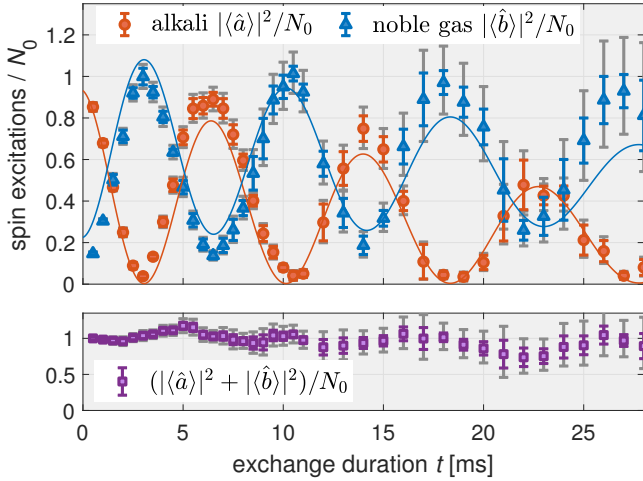


FIG. 2. Exchange of collective spin excitations. Measurement of the coherent exchange between the alkali spin $\langle \hat{a} \rangle$ (red circles) and the noble-gas spin $\langle \hat{b} \rangle$ (blue triangles) in the strong-coupling regime. A short pulse of transverse magnetic field at $t = 0$ excites $N_0 = |\langle \hat{a}(0) \rangle|^2 + |\langle \hat{b}(0) \rangle|^2 = (13.2 \pm 0.6) \cdot 10^{13}$ spins. The experimental conditions at $t = 0$ are $J = 78 \pm 8$ Hz, $\gamma = 6 \pm 1.5$ Hz, and $\Delta = -1.15J$ (for obtaining maximal extinction of $\langle \hat{a} \rangle$ at the minima, see text). Lines present the result of a detailed model using these parameters. Each data-point is averaged over 12 to 20 repetitions of the experimental sequence (shown in Fig. 6). Colored errorbars include uncertainties in the spin-projection measurements and the scattering between repetitions. Gray errorbars also include the uncertainty in the alkali polarization $p_a(t)$, required for converting spin projections to excitations. The bottom panel presents the same data in terms of $|\langle \hat{a} \rangle|^2 + |\langle \hat{b} \rangle|^2$, confirming that the total number of excitations is conserved by the exchange process, up to an overall decoherence.

demonstrate this dynamics, we tune Δ close to resonance and generate an initial excitation predominantly of the alkali spin. Fig. 2 presents the measured spin excitations $|\langle \hat{a} \rangle|^2$ and $|\langle \hat{b} \rangle|^2$, as they are exchanged back and fourth between the two ensembles. Because the magnetic pulse acts also on the noble-gas spin and partially excites it as well, the extinction of $|\langle \hat{a}(t) \rangle|^2$ at the minima of the observed oscillations is maximized slightly below resonance, at $\Delta = -1.15J$; the presented measurement is taken at this detuning. This detuning is still small in terms of the strong-coupling dynamics, rendering a near-unity ratio between the exchange and coupling rates $\tilde{J}/J = 1.15$.

We find that the exchange conserves the total number of excitations $|\langle \hat{a} \rangle|^2 + |\langle \hat{b} \rangle|^2$, which exhibits a roughly monotonic decay due to spin decoherence. We also directly observe the slowing down of the exchange oscillations, as the spins gradually decouple due to the dependence of \tilde{J} on the decaying alkali polarization $p_a(t)$. This gradual decoupling also leads to residual excitations populating the long-lived noble gas spin. These effects are all captured by a detailed model (solid lines), described in Methods, which accounts for the temporal decrease of J and for small geometric misalignments.

It is instructive at this point to compare the resonant, strong-coupling dynamics to the dynamics off resonance or to an overdamped dynamics. These are presented in Fig. 3, showing the measured amplitudes $\text{Re}\langle \hat{a} \rangle$ and $\text{Im}\langle \hat{a} \rangle$ (bottom panel) and total number $|\langle \hat{a} \rangle|^2$ (top panel) of collective alkali spin excitations. For the coherent spin states in our experiment, oscillations of $|\langle \hat{a}(t) \rangle|^2$ correspond to nutations (tilt) of the collective alkali spin from the quantization axis \hat{z} , whereas oscillations of $\langle \hat{a}(t) \rangle$ also include the Larmor precession in the xy plane.

First, we set Δ close to resonance ($\Delta = -1.15J$ as before) and measure the dynamics under the strong-coupling conditions $J = 68 \pm 5$ Hz and $\gamma = 6.5 \pm 2$ Hz (Fig. 3a). As in Fig. 2, we observe oscillations of the number of alkali spin excitations $|\langle \hat{a}(t) \rangle|^2$, exchanged back and forth with the noble-gas spin while gradually decaying. The dynamics far-off resonance is shown for an increased detuning $\Delta = 460$ Hz $\approx 6.8J$ (Fig. 3b). In this regime, we observe a decaying precession of $\langle \hat{a}(t) \rangle$ and an almost monotonic relaxation of $|\langle \hat{a}(t) \rangle|^2$ at a rate 14 ± 2 Hz, in agreement with the expected value (2γ) . Finally, we repeat the experiments with an increased relaxation rate $\gamma = 215$ Hz $\approx 3.2J$ (Fig. 3c), implemented by keeping the pumping beam on during the measurement. No exchange oscillations occur in this regime. The observed relaxation rate is reduced compared to the decoupled case (Fig. 3c, dotted), since here the proximity to resonance $\Delta < \gamma$ leads to dissipative hybridization of the alkali and noble-gas spins, which increases the coherence time of the former, as studied by Kornack *et al.* [3]. The measurements in Fig. 3 of the three regimes elucidate the coherent nature of the exchange interaction under the strong-coupling conditions.

Spectral map

A hallmark of strong coupling is the opening of a spectral gap in the response function of the coupled system at resonance. We measure this gap by repeating the experiment presented in Fig. 3a for different values of Δ . The spectral map, shown in Fig. 4a, reveals an avoidance crossing at $\Delta = 0$ between the normal frequencies, with a wide gap indicating a strong coherent coupling between the two gases. We further compare the measurements to calculated spectra. We present both a simple model based on Eq. (1) (dashed lines in Fig. 4a) and the results of our detailed model (Fig. 4b). Both models reproduce well the main frequency branches. The additional features in the spectrum, primarily the weak perpendicular branches and the vanishing amplitude of the horizontal branch at $\Delta \gtrsim J$ (due to reduced sensitivity to magnetic stimulation near the so-called compensation point [3]) are well captured by the detailed model.

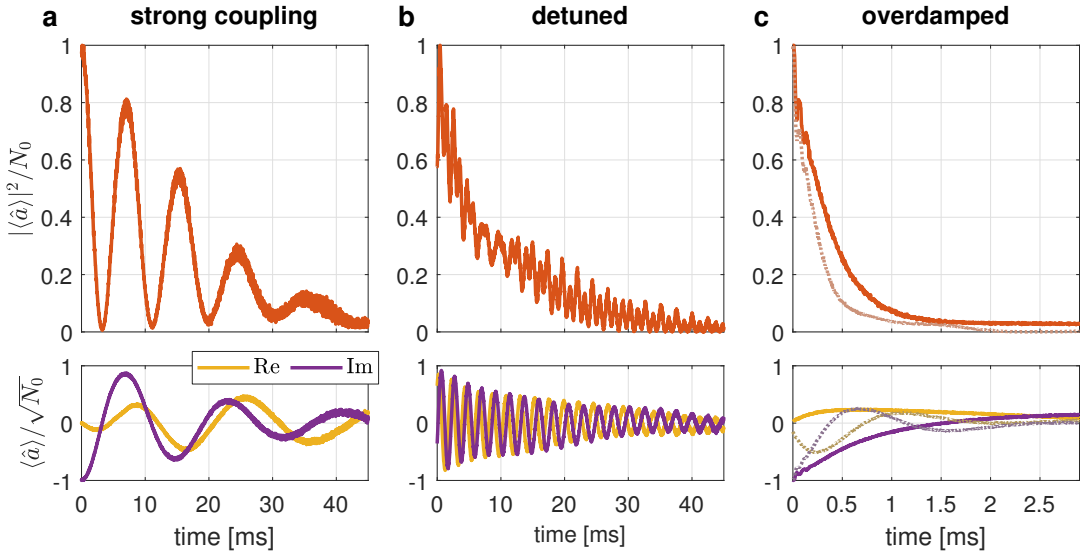


FIG. 3. **Measured dynamics of the coupled alkali-noble-gas spin system in three regimes.** All measurements begin with a short magnetic stimulation of $N_0 = (5.9 \pm 0.4) \cdot 10^{13}$ alkali spin excitations, and the initial alkali-noble-gas coupling rate is $J \approx 68$ Hz. **Top:** Collective spin excitations of the alkali atoms. **Bottom:** Real and imaginary parts of the collective spin amplitude, associated with the two transverse spin components in the lab frame, exhibiting Larmor precession in addition to the exchange. **a. Strong-coupling**, achieved when J exceeds the alkali relaxation rate $\gamma = 0.1J$ and close to resonance $\Delta = -1.15J$. Collapse and revival of alkali spin excitations provide evidence for a coherent hybridization with the noble-gas spins. **b. Decoupled dynamics**, observed when increasing the detuning to $\Delta = 6.8J = 69\gamma$ by increasing the magnetic field. The alkali spin, here largely decoupled from the noble-gas spin, undergoes standard Larmor precession and relaxation. **c. Overdamped dynamics**, obtained under conditions of weak coupling $\gamma = 3.2J$. When near resonance (solid line, $\Delta = -0.15\gamma$), the long-lived noble-gas spin partially hybridizes with the alkali spin, whose relaxation slows down compared to the non-resonant case (dotted line, $\Delta = \gamma$).

DISCUSSION

In summary, we realize a strong coherent coupling between the collective spins of dense alkali vapor and noble gas, relying on stochastic spin-exchange collisions. Each single collision is very weak: the mutual precision angle of the alkali (electron) spin around the noble-gas (nuclear) spin is on average only $\sim 10^{-5}$ radians per collision. Nevertheless, as we show, the collisions can accumulate to an efficient collective coupling. We demonstrate the coherent exchange of excitations between the two spin gases and measure a sizeable avoided-crossing gap in their spectral response when scanning the magnetic field across the resonance. These observations manifest the coherent hybridization of the two collective spins. They attest to the fact that coherence endures the randomness and stochasticity of the collisions, provided that the collisions are individually weak enough, as studied analytically and numerically in Ref. [21].

The strong-coupling regime $J \gg \gamma$ offers a fast reversible interface to noble-gas spins. While reversible manipulations are also possible in the overdamped regime $J \lesssim \gamma$, they are limited to adiabatic operations, slow compared to the coupling rate. We report on $J/\gamma \approx 13$ and estimate that higher values are achievable with higher ${}^3\text{He}$ density and polarization and with lower densities of the alkali and nitrogen gases. ${}^3\text{He}$ pressure exceeding 10 atm was demonstrated [1] as well as 85% polarization [35]. A system at 220 °C with 8.2 atm of

${}^3\text{He}$ polarized to 80% and near unity polarized potassium is expected to achieve $J/\gamma > 100$.

The hybridization of optically-accessible alkali spins and long-lived noble-gas spins opens several intriguing possibilities. One route motivated by quantum information applications is using the alkali spins as mediators between photons and noble-gas spins [34]. The strong spin-spin coupling can improve the performance of such applications by enhancing the indirect coupling to photons. Noble-gas based optical quantum memories, for example, would feature enhanced memory bandwidth when operated in the strong-coupling regime [6]. While memories relying on damped coupling are expected to have a few-Hz bandwidth [18, 19], the memory bandwidth in the strong-coupling regime is essentially independent of J ; light is first stored on the alkali spins (bandwidth > MHz) and subsequently mapped onto the noble-gas spins with efficiency $e^{-(\pi\gamma)/(2J)}$ for hours-long storage [6]. Another example is the generation of long-lived spin-entanglement, which in the strong-coupling regime will benefit from a significant suppression of the contribution of alkali projection noise at elevated alkali densities by a factor $4\gamma/(J^2T)$, where T is the duration of the entangling pulse [5]. A second potential route is utilizing the strong coupling for improving noble-gas-based sensors. Alkali-noble-gas magnetometers, for example, are used as precise gyrometers and as probes for new physics, as they feature high sensitivity to anomalous fields and to bosonic dark matter [13, 16].

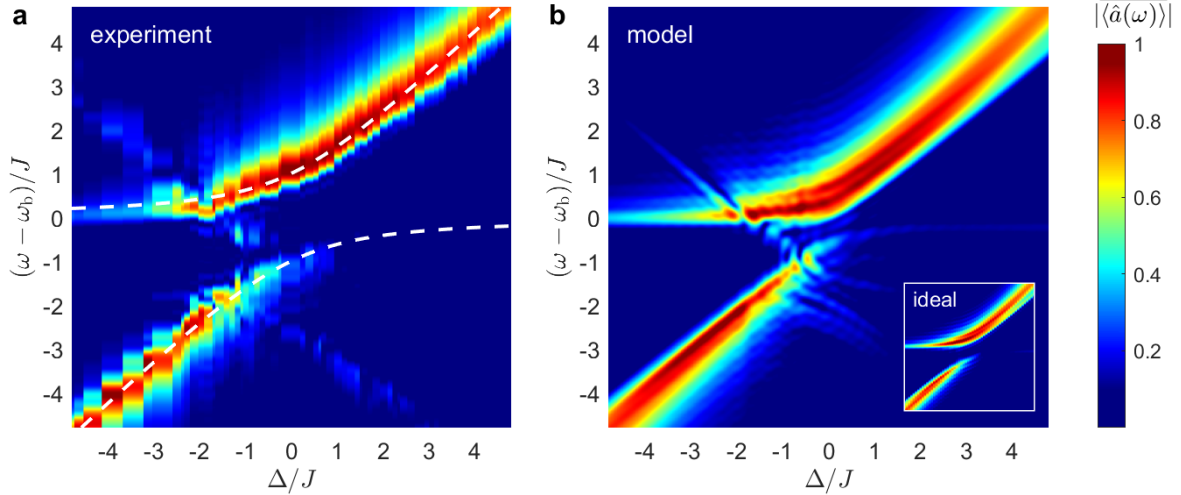


FIG. 4. Spectral response of the alkali-noble-gas spin system in the strong coupling regime. **a.** Measured response of the collective alkali spin $\langle \hat{a} \rangle$ to a weak stimulation, for different detunings between the spins Δ . The spectrum $\langle \hat{a}(\omega) \rangle \propto \int_0^\infty \langle \hat{a}(t) \rangle e^{-i\omega t} dt$ (normalized separately for each Δ , see Methods) manifests the eigenvalues of the coupled system; The spectrum maxima correspond to the normal frequencies, and the spectral widths are indicative of the decay. Dashed lines are the imaginary part of the eigenvalues of Eq. (1). A clear avoided crossing with a sizeable spectral gap at $|\Delta| < J$ indicates the strong, coherent hybridization of the two spin gases. The response at $|\Delta| > J$ corresponds to the independent precession rates of the alkali and noble-gas spins ω_a and ω_b respectively. The axes are scaled by the average value $J = 47$ Hz (rather than the initial value $J = 79$ Hz) to account for the decrease of J due to alkali depolarization during the 65-ms-long measurement. **b.** Calculated spectral response from a detailed model. The model includes a misalignment of 3.1 mrad between the magnetic field and the pumping direction; Inset shows the model results without this misalignment.

These sensors however have a relatively slow response time, typically limited by $\gamma/2$ close to resonance. A strong coupling in these sensors could enhance their bandwidth up to J while maintaining their high sensitivity.

MATERIALS AND METHODS

The Holstein-Primakoff transformation from spins to bosonic excitations

The states of the alkali and noble-gas spin ensembles are characterized by their degree of polarization $p_a = (2/N_a) \sum_m \langle \hat{s}_z^{(m)} \rangle$ and $p_b = (2/N_b) \sum_n \langle \hat{k}_z^{(n)} \rangle$. Here, $\sum_m \hat{s}_j^{(m)}$ and $\sum_n \hat{k}_j^{(n)}$ with $j = \{x, y, z, -, +\}$ are the standard collective spin operators of the electrons of the alkali atoms and the nuclei of the noble gas atoms, respectively, and $N_a = n_a V$ and $N_b = n_b V$ are the number of atoms in the volume V . Describing the alkali spins in terms of only the electronic spins is possible owing to the frequent alkali-alkali collisions, which constantly drive the alkali atoms to a spin-temperature distribution [36]. In the spin-temperature distribution, due to the hyperfine coupling to the alkali nuclear spin, the spin precession around an external magnetic field is slower than that of a bare electron by a factor $q(p_a)$, known as the slowing-down factor; for potassium, $q(p_a) = 2 + 4/(1 + p_a^2)$ [36–38].

We are interested in the bosonic annihilation operators

\hat{a} and \hat{b} , defined according to the Holstein-Primakoff transformation as $\hat{a} = \sqrt{q/N_a p_a} \sum_m \hat{s}_-^{(m)}$ and $\hat{b} = \sqrt{1/N_b p_b} \sum_n \hat{k}_-^{(n)}$ [21, 22]. These are the canonical, normalized version of the collective spin operators transverse to the quantization axis. For the alkali spins, we denote the depolarization rate by Γ_1 (decay rate of $p_a = \sum_m \langle \hat{s}_z^{(m)} \rangle$) and the transverse relaxation rate by Γ_2 (decay rate of $\sum_m \langle \hat{s}_x^{(m)} \rangle$ and $\sum_m \langle \hat{s}_y^{(m)} \rangle$). The decoherence rate of the excitations $\langle \hat{a} \rangle$ is therefore given by $\gamma = \Gamma_2 - \Gamma_1/2$, neglecting small variations of q on short timescales.

Apparatus and experimental conditions

We use a spherical cell with diameter $\ell = 2.54$ cm and volume $V = 8.6 \text{ cm}^3$, made of GE-180 aluminosilicate glass, containing ^3He gas, a droplet of natural abundant potassium, and 50 Torr of nitrogen. The temperature of the cell $T = 230^\circ\text{C}$ is maintained using a pair of resistance twisted wires wrapped around an alumina body, which are driven with current oscillating at 320 kHz. The magnetic field is applied via three sets of coils: 4-winding double Helmholtz coils for controlling $B\hat{z}$ and a bird-cage coil for the transverse fields to improve magnetic uniformity. The coils are placed inside five concentric layers of μ -metal magnetic shields, and the inner two layers are degaussed.

The $N_a = 4.2 \cdot 10^{15}$ potassium atoms are polarized by optical pumping using 500 mW of circularly-polarized light at

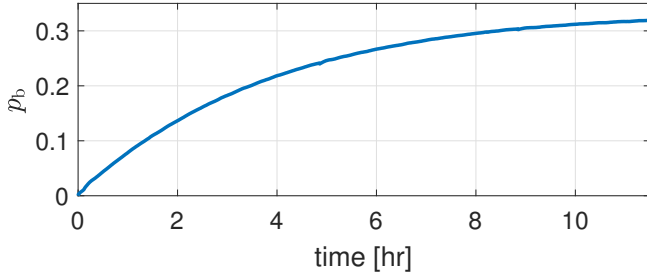


FIG. 5. **Spin-exchange optical pumping.** Typical measurement of the pumping process of helium-3 by optically pumped potassium vapor. Here the potassium density is $n_a = 4.9 \cdot 10^{14} / \text{cc}$, and the helium depolarization time is $T_{1,\text{act}}^b = 3.9$ hours.

770 nm. This pumping light is generated using a free-running diode laser followed by a tapered amplifier. We tune the laser near the optical D1 transition, which in our setup appears as a single absorption line with a full width of 32 GHz due to pressure broadening, producing an on-resonance optical depth of $n_a \sigma_{\text{abs}} \ell \approx 220$ ($\sigma_{\text{abs}} = 1.76 \cdot 10^{-13} \text{ cm}^2$ is the absorption cross-section of the 32-GHz-wide line). The pumping beam is Gaussian with a 25-mm waist diameter. We detune it from resonance to reduce its depletion and by that achieve the high degree of spin polarization $p_a \geq 0.95$.

The depolarization rate of the potassium spins in the dark $\Gamma_1 = 8.6$ Hz is dominated by spin-destruction collisions among potassium atoms and by spin-rotation interaction of potassium atoms with the buffer gas [39]. Rapid spin-exchange collisions among potassium atoms at a rate $R_{\text{se}} = 86$ kHz and the operation at low Larmor precession rates $|\omega_a| \ll \sqrt{R_{\text{se}} \Gamma_1}$ puts the potassium in the so-called spin-exchange relaxation-free (SERF) regime [37, 40], rendering the relaxation induced by spin-exchange collisions negligible. Consequently, the transverse spin relaxation rate $\Gamma_2 = 10.3$ Hz is dominated by the depolarization processes, with minor contribution from magnetic inhomogeneity. These lead to a decoherence rate of $\gamma = \Gamma_2 - \Gamma_1/2 \approx 6$ Hz for the bosonic excitations of the potassium spins.

The $N_b = 5.5 \cdot 10^{20}$ helium atoms are hyperpolarized using spin-exchange optical pumping (SEOP) [36] at a rate $(3.6 \pm 0.3) \cdot 10^{-6}$ Hz in the presence of an axial magnetic field $B = 400$ mG. A typical SEOP measurement settling at $p_b \geq 0.3$ is presented in Fig. 5. In our system, at low temperature, the measured depolarization and decoherence times of the helium spins $T_1^b = 22$ hours and $T_2^b = 2$ hours are limited by magnetic field inhomogeneity within the cell volume. At elevated temperature and polarizations, we measure $T_{1,\text{act}}^b = 3.9$ hours (see Fig. 5) due to inhomogeneity of the magnetizations of the two ensembles in the cell, which slightly deviates from an ideal sphere [41]. To moderate the helium depolarization during the experiments, we intermittently turn on the SEOP in between measurements.

The polarized spin ensembles exert an equivalent magnetic field (EMF) on each other, via collisions and via the macroscopic magnetic fields generated by their

magnetization. While the EMF experienced by the helium $B_{a \rightarrow b} = -0.24$ mG (for $p_a = 0.98$) is small, the EMF experienced by the potassium $B_{b \rightarrow a} = -10.94$ mG (for $p_b = 0.3$) is considerable. The detuning from resonant coupling Δ is thus quite sensitive to p_b , which we monitor during the experiment. We do so by applying a constant magnetic field $-B_{b \rightarrow a} + 1.6$ mG, and monitoring the precession frequency of the decoupled alkali spins following a small transverse magnetic pulse.

In the experiments presented in Fig. 2, Fig. 3, and Fig. 4, we use a transverse magnetic pulse to tilt the alkali spins by $\theta_a = 9.8 \pm 0.2^\circ$, $\theta_a = 6.8 \pm 0.2^\circ$, and $\theta_a = 0.7 \pm 0.05^\circ$, respectively. In terms of the number of excitations $|\langle \hat{a} \rangle|^2 = q N_a p_a \theta_a^2 / 4$, these correspond to $|\langle \hat{a} \rangle|^2 = (12.1 \pm 0.5) \cdot 10^{13}$, $|\langle \hat{a} \rangle|^2 = (5.9 \pm 0.4) \cdot 10^{13}$, and $|\langle \hat{a} \rangle|^2 = (6.2 \pm 0.9) \cdot 10^{11}$.

In all experiments, we measure the transverse spin component of the alkali atoms along the \hat{x} axis using Faraday rotation of a linearly-polarized probe beam. The 5-mm diameter, $260 \mu\text{W}$, probe beam is detuned by ~ 400 GHz above the D1 transition and its polarization is measured after the cell using balanced photodetection method [42]. We subtract from all measurements a background signal taken without the magnetic pulse. This background signal is small and is dominated by excitations of transverse spins during the fast variation of $B \hat{z}$ (when setting Δ), due to imperfect alignment between the optical and magnetic axes.

Reconstruction and scaling of $\langle \hat{a} \rangle$ and $\langle \hat{b} \rangle$

We use optical Faraday rotation to measure $\langle \hat{a} \rangle$ and $\langle \hat{b} \rangle$. For the optically-broadened line and the far-detuned probe in our setup, and as long as the Faraday-rotation angle is small, the balanced-detection readout is proportional to the \hat{x} axis of the collective alkali spin $\langle \sum_m \hat{s}_x^{(m)} \rangle$, *i.e.*, to the electron spin projection along the probing axis [43]. From these measurements we extract the normalized transverse spin component $\bar{S}_x(t) = \langle \sum_m \hat{s}_x^{(m)}(t) \rangle / [N_a p_a(0)/2]$. The normalization factor is calibrated separately by tilting the initial spin $[N_a p_a(0)/2] \hat{z}$ all the way to the \hat{x} direction (equivalent to $\theta_a = 90^\circ$) and measuring the maximal Faraday rotation angle (~ 4 radian in our system). We verify that the Faraday rotation angle in all subsequent experiments is small.

The measurements of $|\langle \hat{a}(t) \rangle|^2$ and $|\langle \hat{b}(t) \rangle|^2$ presented in Fig. 2 are done according to the experimental sequence shown in Fig. 6a. The sequence starts by initializing the spins with a small transverse component under conditions of small Δ . After some evolution and partial decay in the dark, at time t , we increase Δ by an order of magnitude (by increasing $B + B_{b \rightarrow a}$ to 1.5 mG), thus largely decoupling the alkali and noble-gas spins. We continue to monitor the alkali spins and use them as a magnetometer for sensing the noble-gas spins.

During the experiment, when the pumping light is off, the polarization of the alkali spin decays $p_a(t) \leq p_a(0)$. This decay, which is to leading order exponential with decay rate Γ_1 , changes the slowing-down factor $q(t) = q[p_a(t)]$ and

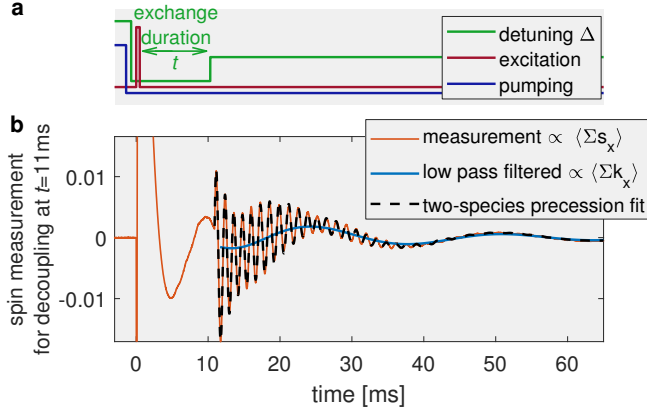


FIG. 6. Pulse sequence and typical results of an excitation-exchange measurement. **a.** First, we turn off the pumping and bring the two species to strong coupling with a small detuning Δ . We then generate a transverse excitation with a pulse of transverse magnetic field. At a later time t , we halt the exchange by increasing the axial magnetic field and setting a large Δ . **b.** Example of a measured signal with exchange duration $t = 11$ ms, with $\Delta = -1.15J$ before t , and $\Delta = 790$ Hz $\gg J$ after t . We measure the alkali electron spin (red) which, once Δ is increased, can be used as a magnetometer that senses the noble-gas spin. The fast oscillations of the signal correspond to the Larmor precession of the alkali spin, and the slow modulation correspond to the noble-gas precession. The latter is highlighted by the blue line (generated by low-pass filtering of the signal for illustrative purposes). We fit the signal to the model from Eq. (3) (dashed black line) and find the amplitudes of the alkali and noble-gas components at time t , which are used to estimate $\langle \hat{a}(t) \rangle$ and $\langle \hat{b}(t) \rangle$, respectively. The same fit also provides $p_a(t)$.

thus shifts the Larmor precession frequency of the alkali spin. Denoting τ as the time elapsed from the decoupling time t , the instantaneous precession frequency of the alkali spin is given by

$$\omega_a(\omega_0, p_a(t), \Gamma_1; \tau) = \frac{2\omega_0}{1 + 2/[1 + p_a^2(t)e^{-2\Gamma_1\tau}]}, \quad (2)$$

where $\omega_0 = \omega_a(p_a = 1; \tau = 0)$. To each measured signal \bar{S}_x , we therefore fit the model

$$\begin{aligned} \bar{S}_x(t + \tau) = \text{Re} & \left[\sigma_a(t) e^{i \int_0^\tau \omega_a(\omega_0, p_a(t), \Gamma_1; \tau') d\tau' - \gamma_a \tau} \right. \\ & \left. + \sigma_b(t) e^{(i\omega_b - \gamma_b)\tau} \right]. \end{aligned} \quad (3)$$

Here $\sigma_a(t)$, $\sigma_b(t)$ are complex fitting parameters, corresponding to the amplitudes of the two frequency components, and γ_a , γ_b , ω_0 , ω_b , $p_a(t)$ are real fitting parameters. One such fit is demonstrated in Fig. 6b, and the extracted $p_a(t)$, $\omega_a(t, \tau = 0)$, $|\sigma_a(t)|^2$, and $|\sigma_b(t)|^2$ are shown in Fig. 7 [note the factor $|\sigma_b/\sigma_a|^2 \approx (J/\Delta)^2 \approx 1/100$]. The value $\Gamma_1 = 8.6$ Hz is set in Eq. (3) for all fits, and it is (self) consistent with $\Gamma_1 = 8.6 \pm 0.5$ Hz extracted from Fig. 7a. Deviations from a pure exponential decay in Fig. 7b at $t > 20$ ms can be attributed to multi-mode spatial dynamics [23], to SEOP of the alkali by the noble gas, and to low signal-to-noise ratios.

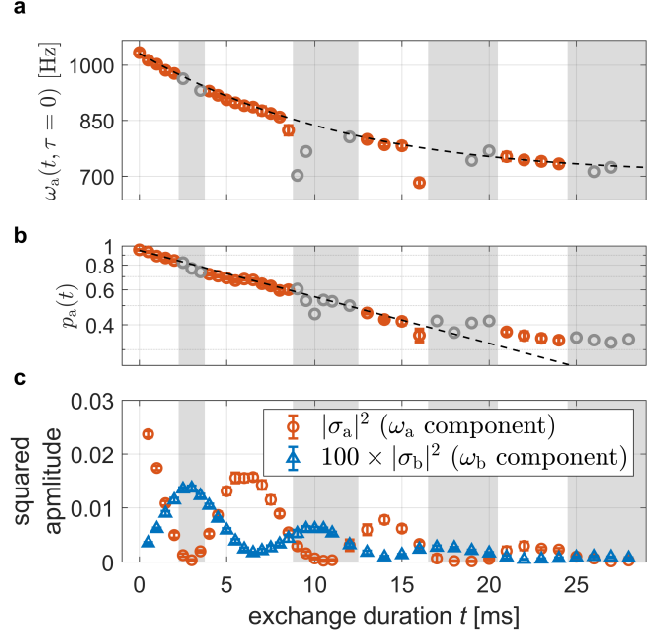


FIG. 7. Variables extracted from fitting Eq. (3) to the measured signals for each exchange time t , as exemplified in Fig. 6. **a.** The change in alkali precession frequency $\omega_a(t, \tau = 0)$ [see Eq. (2)] manifests the change in the slowing-down factor due to alkali depolarization. **b.** The degree of alkali polarization $p_a(t)$ (in semi-log scale). In **a** and **b**, dashed black lines correspond to an exponential decay of $p_a(t)$ at the rate $\Gamma_1 = 8.6$ Hz. Less reliable data, extracted when the excitations reside predominantly in the noble-gas spins, are marked in gray. **c.** The two frequency components (amplitude squared) of the normalized Faraday rotation signal $\bar{S}_x(t + \tau)$. Note the factor of $(\Delta/J)^2 \gtrsim 100$ between them. Each data-point is averaged over 12 to 20 repetitions of the sequence.

With $p_a(t)$ at hand, we obtain the factor $\eta(t) = \frac{N_a q[p_a(t)] p_a^2(0)}{4 p_a(t)}$ between the number of alkali excitations and \bar{S}_x^2 . The alkali and noble-gas excitations presented in Fig. 2 are then given by $|\langle \hat{a}(t) \rangle|^2 = \eta(t) |\sigma_a(t) + \sigma_b(t)|^2$ and $|\langle \hat{b}(t) \rangle|^2 = \eta(t) \left| \frac{\Delta(t)}{J(t)} \sigma_b(t) - \frac{J(t)}{\Delta(t)} \sigma_a(t) \right|^2$, where $\Delta(t) = \omega_a(t, \tau = 0) - \omega_b$ and $J(t) = \sqrt{\frac{p_a(t)}{p_a(0)} \frac{q_a(0)}{q_a(t)}} J(t = 0)$. These expression neglect terms of order $(J/\Delta)^2$ and higher. For the experiments presented in Figs. 3 and 4, we reconstruct the complex-valued $\langle \hat{a}(t) \rangle = \sqrt{\eta(t)} [\bar{S}_x(t) - i \bar{S}_y(t)]$. The two normalized projections $\bar{S}_x(t)$ and $\bar{S}_y(t)$ are measured in two consecutive experiments that differ in the direction of the initial pulsed excitation (alternating between $B_\perp \hat{y}$ and $B_\perp \hat{x}$). We use the $p_a(t) = p_a(0) e^{-\Gamma_1 t}$ for Figs. 3a and 3b and estimate $p_a = p_a(t = 0) = 0.98$ for Fig. 3c. Finally, in Fig. 4 we present the normalized Fourier amplitudes $|\langle \hat{a}(\omega) \rangle| = |\int_0^\infty \langle \hat{a}(t) \rangle dt| / \sqrt{T \int_0^\infty |\langle \hat{a}(t) \rangle|^2 dt}$, where $T = 65$ ms is the sequence duration.

Detailed model

Equation (1) describes idealized dynamics of the spin gases. For the calculations presented in Figs. 2 and 4b, we use a detailed model, which includes the decay of the alkali polarization $p_a = p_a(t)$ during the experimental sequence, the dependence of Δ on $p_a(t)$ via the slowing-down factor $q[p_a(t)]$, misalignment of the optical and magnetic axes, and residual transverse magnetic fields.

The model assumes both spin ensembles are polarized along $-\hat{z}$. It follows Refs. [21, 36] and describes the dynamics of the collective spin excitations $S_- = \sum_m \langle \hat{s}_-^{(m)} \rangle$ and $K_- = \sum_n \langle \hat{k}_-^{(n)} \rangle$, coupled by the Fermi-contact interaction occurring during stochastic collisions. In the presence of axial magnetic field $B\hat{z}$ and transverse magnetic field $B_- = B_x - iB_y$, the coupled spin equations are given by

$$\begin{aligned} \partial_t S_- &= i(\omega_a + i\Gamma_2)S_- - i\frac{n_a}{qn_b}J_a K_- + i\frac{g_e}{q}\frac{N_a p_a}{2}B_-, \\ \partial_t K_- &= -i\frac{qn_a}{n_b}J_b S_- + i\omega_b K_- + ig_b\frac{N_b p_b}{2}B_-. \end{aligned} \quad (4)$$

Here $J_a = \sqrt{q}\tilde{\zeta}n_b p_a/2$ and $J_b = \tilde{\zeta}n_a p_b/2\sqrt{q}$ are the uni-directional coupling rates, eventually composing the bi-directional rate $J = \sqrt{J_a J_b}$, with $\tilde{\zeta} = (2 \cdot 10^{-14} \text{ cm}^3/\text{s})/\sqrt{q}$. The gyromagnetic ratios of the electron and helium-3 spins are $g_e = 2.8 \cdot 10^6 \text{ Hz/G}$ and $g_b = -3.27 \cdot 10^3 \text{ Hz/G}$, and the precession frequencies are $\omega_a = g_e B/q + \tilde{\zeta}n_b p_b/2\sqrt{q}$ and $\omega_b = g_b B + \sqrt{q}\tilde{\zeta}n_a p_a/2$.

We simulate the experimental sequences by numerically solving these equations. From the simulation results, we calculate the expectation values $\langle \hat{a} \rangle = \sqrt{q[p_a(t)]/N_a p_a(t)}S_-(t)$ and $\langle \hat{b} \rangle = \sqrt{1/N_b p_b}K_-(t)$. For the model parameters, we use known constants or the measured values from the calibration experiments. For the alkali polarization, we use $p_a(t) = p_a(0)e^{-\Gamma_1 t}$ with $\Gamma_1 = 8.6 \text{ Hz}$ and $p_a(0) = R_p/(R_p + \Gamma_1) = 0.98$, where $R_p = 430 \text{ Hz}$ is the optical pumping rate. For the noble-gas polarization, we set $p_b = n_a k_{\text{se}} p_a(0)T_{1,\text{act}}^b = 0.32$ due to SEOP, where $k_{\text{se}} = 5.5 \cdot 10^{-20} \text{ cm}^3/\text{s}$ is the SEOP rate.

The model can account for various geometric misalignments and other experimental imperfections: (1) Misalignment of the pumping beam from the \hat{z} axis generates an initial transverse spin component. If the pumping beam points towards $\eta_x \mathbf{e}_x + \eta_y \mathbf{e}_y + \mathbf{e}_z$ (given $\eta_{x,y} \ll 1$), the initial value of S_- is $N_a p_a(t=0)(\eta_x - i\eta_y)/2$. (2) A residual magnetic field pointing towards $\beta_x \mathbf{e}_x + \beta_y \mathbf{e}_y + \mathbf{e}_z$ (given $\beta_{x,y} \ll 1$) during the SEOP process would turn the initial value of K_- to $N_b p_b(\beta_x - i\beta_y)/2$. (3) A non-vanishing transverse magnetic field during the sequences can be accounted for by a constant offset of B_- . When varying Δ during the sequence, these misalignments could tilt the spins and introduce spurious (background) excitations. (4) A misalignment of the probe field can be accounted for by extracting the signal $S = \text{Re}(1 + i\varepsilon_{\parallel})S_- + \varepsilon_{\perp}N_a p_a/2$ for

$\varepsilon_{\parallel,\perp} \ll 1$ (rather than simply $S = S_-$) from the simulation results.

We calculate the spectral map presented in Fig. 4b by repeating the calculation for $10.6 \text{ mG} < B < 11.8 \text{ mG}$ (corresponding to $-5 < \Delta/J < 5$). The excitation is simulated by applying $B_{\perp}(t) = 2.4 \text{ mG} \times \exp[-t^2/(2.8 \mu\text{s})^2]$ ($\theta_a = 3^\circ$). We calculate the Fourier transform of $\langle \hat{a} \rangle$ and the normalized amplitude $|\langle \hat{a}(\omega) \rangle|$, as done for the experimental data. We reproduce the imperfection generating the perpendicular frequency branch by introducing a minute misalignment $\beta_x = \beta_y = 2.2 \text{ mrad}$ (and $\eta_x = \eta_y = \varepsilon_{\parallel} = \varepsilon_{\perp} = 0$). The inset of Fig. 4b is calculated with $\beta_x = \beta_y = 0$. The calculations for Fig. 2a (solid lines) are done with $B = 11.33 \text{ mG}$ ($\Delta = -1.15J$) and $B_{\perp}(t) = 5.2 \text{ mG} \times \exp[-t^2/(2.8 \mu\text{s})^2]$ ($\theta_a = 6.5^\circ$).

ACKNOWLEDGMENTS:

We thank Chen Avinadav and Ran Finkelstein for fruitful discussions. We acknowledge financial support by the Israel Science Foundation, the European Research Council starting investigator grant Q-PHOTONICS 678674, the Minerva Foundation with funding from the Federal German Ministry for Education and Research, and the Laboratory in Memory of Leon and Blacky Broder.

* These authors contributed equally to this work.

- [1] T. R. Gentile, P. J. Nacher, B. Saam, and T. G. Walker, *Reviews of Modern Physics* **89**, 045004 (2017).
- [2] T. G. Walker and M. S. Larsen, *Advances in Atomic Molecular and Optical Physics* **65**, 373 (2016).
- [3] T. W. Kornack and M. V. Romalis, *Physical Review Letters* **89**, 253002 (2002).
- [4] R. Jiménez-Martínez, D. J. Kennedy, M. Rosenbluh, E. A. Donley, S. Knappe, S. J. Seltzer, H. L. Ring, V. S. Bajaj, and J. Kitching, *Nature Communications* **5**, 3908 (2014).
- [5] O. Katz, R. Shaham, E. S. Polzik, and O. Firstenberg, *Physical Review Letters* **124**, 043602 (2020).
- [6] O. Katz, E. Reches, R. Shaham, A. V. Gorshkov, and O. Firstenberg, *arXiv:2007.08770* (2020).
- [7] W. Heil, C. Gemmel, S. Karpuk, Y. Sobolev, K. Tullney, F. Allmendinger, U. Schmidt, M. Burghoff, W. Kilian, S. Knappe-Grüneberg, et al., *Annalen der Physik* **525**, 539 (2013).
- [8] C. Gemmel, W. Heil, S. Karpuk, K. Lenz, C. Ludwig, Y. Sobolev, K. Tullney, M. Burghoff, W. Kilian, S. Knappe-Grüneberg, et al., *The European Physical Journal D* **57**, 303 (2010).
- [9] T. W. Kornack, R. K. Ghosh, and M. V. Romalis, *Physical Review Letters* **95**, 230801 (2005).
- [10] D. A. Thrasher, S. S. Sorensen, J. Weber, M. Bulatowicz, A. Korver, M. Larsen, and T. G. Walker, *Physical Review A* **100**, 061403 (2019).
- [11] J. Kitching, *Applied Physics Reviews* **5**, 031302 (2018).
- [12] T. Chupp and S. Swanson, *Advances in Atomic Molecular and Optical Physics* **45**, 41 (2001).

- [13] J. M. Brown, S. J. Smullin, T. W. Kornack, and M. V. Romalis, Physical Review Letters **105**, 151604 (2010).
- [14] D. F. Jackson Kimball, A. Boyd, and D. Budker, Physical Review A **82**, 062714 (2010).
- [15] R. Alonso, D. Blas, and P. Wolf, Journal of High Energy Physics **2019**, 69 (2019).
- [16] I. M. Bloch, Y. Hochberg, E. Kuflik, and T. Volansky, J. High Energy Phys. **2020**, 167 (2020).
- [17] T. E. Chupp, P. Fierlinger, M. J. Ramsey-Musolf, and J. T. Singh, Reviews of Modern Physics **91**, 015001 (2019), 1710.02504.
- [18] O. Katz, R. Shaham, E. Reches, A. V. Gorshkov, and O. Firstenberg, arXiv:2007.10177 (2020).
- [19] A. Dantan, G. Reinaudi, A. Sinatra, F. Laloë, E. Giacobino, and M. Pinard, Physical Review Letters **95**, 123002 (2005).
- [20] A. Serafin, M. Fadel, P. Treutlein, and A. Sinatra, arXiv:2012.07216 (2020).
- [21] O. Katz, R. Shaham, and O. Firstenberg, arXiv:1905.12532 (2019).
- [22] K. Hammerer, A. S. Sørensen, and E. S. Polzik, Reviews of Modern Physics **82**, 1041 (2010).
- [23] R. Shaham, O. Katz, and O. Firstenberg, Physical Review A **102**, 012822 (2020).
- [24] J. Sun, X. Zhang, W. Qu, E. E. Mikhailov, I. Novikova, H. Shen, and Y. Xiao, Phys. Rev. Lett. **123**, 203604 (2019).
- [25] A. T. Dellis, M. Loulakis, and I. K. Kominis, Physical Review A **90**, 032705 (2014).
- [26] J. Kong, R. Jiménez-Martínez, C. Troullinou, V. G. Lucivero, G. Toth, and M. W. Mitchell, Nat. Commun. **11** (2020), ISSN 2041-1723.
- [27] K. Mouloudakis and I. K. Kominis, Physical Review A **103**, L010401 (2021).
- [28] J. F. Sherson, H. Krauter, R. K. Olsson, B. Julsgaard, K. Hammerer, I. Cirac, and E. S. Polzik, Nature **443**, 557 (2006).
- [29] A. V. Gorshkov, A. André, M. Fleischhauer, A. S. Sørensen, and M. D. Lukin, Physical Review Letters **98**, 123601 (2007).
- [30] O. Firstenberg, P. London, D. Yankelev, R. Pugatch, M. Shuker, and N. Davidson, Physical review letters **105**, 183602 (2010).
- [31] S. Appelt, A. B. Baranga, C. J. Erickson, M. V. Romalis, A. R. Young, and W. Happer, Physical Review A **58**, 1412 (1998).
- [32] M. Batz, P. J. Nacher, and G. Tastevin, in Journal of Physics Conference Series (2011), vol. 294, p. 012002.
- [33] D. K. Walter, W. Happer, and T. G. Walker, Physical Review A **58**, 3642 (1998).
- [34] O. Katz, R. Shaham, and O. Firstenberg, arXiv:2102.00229 (2021).
- [35] W. C. Chen, T. R. Gentile, Q. Ye, T. G. Walker, and E. Babcock, Journal of Applied Physics **116**, 014903 (2014).
- [36] T. G. Walker and W. Happer, Reviews of Modern Physics **69**, 629 (1997).
- [37] J. C. Allred, R. N. Lyman, T. W. Kornack, and M. V. Romalis, Physical Review Letters **89**, 130801 (2002).
- [38] G. Vasilakis, V. Shah, and M. V. Romalis, Physical Review Letters **106**, 143601 (2011).
- [39] W. Happer, Y.-Y. Jau, and T. Walker, Optically Pumped Atoms (WILEY-VCH, 2010), ISBN 978-3-527-40707-1.
- [40] W. Happer and A. C. Tam, Physical Review A **16**, 1877 (1977).
- [41] M. V. Romalis, D. Sheng, B. Saam, and T. G. Walker, Physical Review Letters **113**, 188901 (2014).
- [42] O. Katz, O. Peleg, and O. Firstenberg, Physical Review Letters **115**, 113003 (2015).
- [43] L.-M. Duan, J. I. Cirac, P. Zoller, and E. S. Polzik, Physical Review Letters **85**, 5643 (2000).